Heterogeneous nucleation at a wall near a wetting transition: a Monte Carlo test of the classical theory

2009 J. Phys.: Condens. Matter 21 464118

(http://iopscience.iop.org/0953-8984/21/46/464118)

J. Phys.: Condens. Matter **21** (2009) 464118 (15pp) doi:10.1088/0953-8984/21/46/464118

Heterogeneous nucleation at a wall near a wetting transition: a Monte Carlo test of the classical theory

David Winter, Peter Virnau and Kurt Binder

Institut für Physik, Johannes Gutenberg-Universität, Mainz, Staudinger Weg 7, D-55099 Mainz, Germany

E-mail: kurt.binder@uni-mainz.de

Received 3 April 2009, in final form 14 May 2009
Published 29 October 2009
Online at stacks.iop.org/JPhysCM/21/464118

Abstract

While for a slightly supersaturated vapor the free energy barrier $\Delta F^*_{\rm hom}$, which needs to be overcome in a homogeneous nucleation event, may be extremely large, nucleation is typically much easier at the walls of the container in which the vapor is located. While no nucleation barrier exists if the walls are wet, for incomplete wetting of the walls, described via a nonzero contact angle Θ, classical theory predicts that nucleation happens through sphere-cap-shaped droplets attracted to the wall, and their formation energy is $\Delta F^*_{\rm het} = \Delta F^*_{\rm hom} f(\Theta)$, with $f(\Theta) = (1 - \cos\Theta)^2(2 + \cos\Theta)/4$. This prediction is tested through simulations for the simple cubic lattice gas model with nearest-neighbor interactions. The attractive wall is described in terms of a local 'surface field', leading to a critical wetting transition. The variation of the contact angle with the strength of the surface field is determined by using thermodynamic integration methods to obtain the wall free energies which enter Young's equation. Obtaining the chemical potential as a function of the density for a system with periodic boundary conditions (and no walls), the droplet free energy of a spherical droplet in the bulk is obtained for a wide range of droplet radii. Similarly, $\Delta F^*_{\rm het}$ is obtained for a system with two parallel walls. We find that the classical theory is fairly accurate if a line tension correction for the contact angle is taken into account.

1. Introduction and overview

When one studies the condensation of a vapor induced by a sudden change of external control parameters (e.g. pressure, temperature), the walls of the container may have a pronounced effect on the dynamics of the phase change of the considered fluid. If conditions of 'complete wetting' [1–5] occur, the condensation of the liquid can immediately take place by a growth of the thickness of the liquid wetting layer that coats the wall, and thus the supersaturation of the remaining vapor is immediately removed. Only if the fluid particles are not at all attracted to the walls, so that the latter clearly prefer the vapor phase ('complete drying' of the wall [1–5]), can we expect that condensation in the supersaturated vapor occurs by 'homogeneous nucleation' [6–18] in the bulk of the fluid, and the effect of the walls is negligible. While the situation of complete wetting corresponds to a Young [19] contact angle $\Theta = 0$, complete drying means $\theta = \pi$. However, the most interesting case occurs for the intermediate case of 'incomplete wetting' ($0 < \Theta \leqslant \pi/2$) or 'incomplete drying' ($\pi/2 \leqslant \Theta < \pi$). One readily finds that a sphere-cap-shaped droplet attached to the wall provides a substantial reduction of the free energy barrier against nucleation, in comparison with the free energy barrier $\Delta F^*_{\rm hom}$ that needs to be overcome when in the bulk of the fluid a spherical droplet (with critical droplet radius R^*) is formed [20–22]. According to the classical theory of homogeneous nucleation [12–18], for a weakly supersaturated vapor the free energy cost of forming a liquid droplet can be written as a sum of a volume term ($\propto 4\pi R^3/3$) and a surface term ($\propto 4\pi R^2$)

$$\Delta F(R) = -\Delta\mu(\rho_\ell - \rho_v)\left(\frac{4\pi R^3}{3}\right) + \gamma_{v\ell} 4\pi R^2. \quad (1)$$

$\Delta\mu$ is the chemical potential difference relative to the coexistence value $\Delta\mu = \mu - \mu_{\rm coex}(T)$, and ρ_ℓ, ρ_v are the densities of the coexisting liquid (ρ_ℓ) and vapor (ρ_v) phases. Here it was assumed that the supersaturation of the metastable

vapor is small enough, so that the pressure difference between the droplet and the surrounding vapor can be expanded linearly in $\Delta\mu$. In the surface term, $\gamma_{v\ell}$ denotes the surface tension of a flat vapor–liquid interface, and hence is independent of both R and $\Delta\mu$ ('capillarity approximation'). As it is well known, (1) leads to a critical droplet radius R^* (where $\partial\Delta F(R)/\partial R = 0$) and associated free energy barrier $\Delta F^*_{\rm hom}$

$$R^* = 2\gamma_{v\ell}/[\Delta\mu(\rho_\ell - \rho_v)],$$
$$\Delta F^*_{\rm hom} = \frac{16\pi}{3}\{\gamma^3_{v\ell}/[\Delta\mu(\rho_\ell - \rho_v)]^2\}. \quad (2)$$

Now we consider a system with walls where at coexistence a macroscopically large liquid droplet is attached to the wall. The droplet exhibits the contact angle Θ, which is related to the wall–vapor ($\gamma_{\rm wv}$) and wall–liquid ($\gamma_{w\ell}$) surface tensions by Young's equation [9]

$$\gamma_{v\ell}\cos\Theta = \gamma_{\rm wv} - \gamma_{w\ell}. \quad (3)$$

The extension of the classical theory ((1) and (2)) due to Turnbull [20–22] yields a free energy barrier $\Delta F^*_{\rm het}$ against heterogeneous nucleation which is reduced in comparison with $\Delta F^*_{\rm hom}$ by a factor given solely by the contact angle, $f(\Theta)$,

$$\Delta F^*_{\rm het} = \Delta F^*_{\rm hom} f(\Theta),$$
$$f(\Theta) = (1-\cos\Theta)^2(2+\cos\Theta)/4. \quad (4)$$

In addition to the assumptions made for the derivation of (2), it is further assumed that the dependence of $\gamma_{\rm wv}$, $\gamma_{w\ell}$ on $\Delta\mu$ is negligible. Line tension [23–38] effects are disregarded too, which lead to a correction to (3) as follows [34–36]

$$\gamma_{v\ell}\cos\Theta = \gamma_{\rm wv} - \gamma_{w\ell} + \tau\kappa^*. \quad (5)$$

Here, τ is the line tension and κ^* is the geodesic curvature of the contact line (which is a circle for a sphere-cap-shaped droplet). We note, however, that for small droplets (where (5) seems to make a substantial correction, as simulations of sessile droplets have indicated [39]) one also expects a curvature correction to $\gamma_{\ell v}$ [40], involving the 'Tolman length' δ,

$$\gamma_{v\ell}(R) = \gamma_{v\ell}/(1+2\delta/R). \quad (6)$$

However, the physical meaning and properties of this length are still under discussion (see [41] and references therein). Recent attempts to find $\gamma_{v\ell}(R)$ from Monte Carlo simulations of a Lennard-Jones fluid [42, 43] yielded a $\gamma(R)$ inconsistent with (6).

At this point, we emphasize that the experimental evidence for the validity of (4) is scarce, if at all existent. As it is well known, accurate measurements of nucleation rates J (which are related to ΔF^* via $J = \nu^* \exp(-\Delta F^*/k_{\rm B}T)$ where the pre-exponential factor ν^* incorporates all kinetic aspects of droplet growth) are notoriously difficult [12, 17, 18, 44]. Critical droplets are nanoscopically small and very rare. Their direct experimental observation is thus elusive. The rate of nucleation can only be inferred indirectly from the stage where the nuclei have grown to a much larger size, at which they are observable, i.e., one can only study the combined effect of nucleation and growth. It is often difficult to distinguish between homogeneous and heterogeneous mechanisms (the latter may be due to ions [45] and nanoscopically small dust or aerosol particles [46] in the vapor, not only due to the walls of the container). Quantitatively accurate measurements of contact angles Θ of droplets at flat walls are also difficult [1–3, 47–49], due to hysteresis between advancing and receding contact angles caused by the substrate surface roughness, contact line pinning at impurities, etc. Again, the direct experimental observation of nanoscopically small droplets at walls is a nontrivial task. As a result, comprehensive experimental tests of (4) have, to our knowledge, not been possible so far. One can even find in the literature the statement that 'the understanding of heterogeneous nucleation processes is rather poor' (e.g. [50], p 489). Studies of heterogeneous nucleation by more refined theories such as density functional theories (e.g. [51–55]) or computer simulations (e.g. [56–62]) are also scarce and do not give an exhaustive solution to the problems discussed above. Nevertheless the few results that do exist already indicate that line tension effects are very important (e.g. [58, 59]). In the present work we make a contribution to this problem of droplet formation at walls near wetting transitions by a study of the Ising (lattice gas) model. For the study of homogeneous nucleation in the bulk, the Ising model has already played a key role [14, 15, 63–71]: due to particle–hole symmetry, the chemical potential at coexistence $\mu_{\rm coex}$ is exactly known, unlike off-lattice fluids where $\mu_{\rm coex}$ is only known within some error. The 'order parameter' $\rho_\ell - \rho_v$ and interface free energy at coexistence $\gamma_{v\ell}$ are also known exactly in $d = 2$ dimensions [72] and numerically in $d = 3$ dimensions with high precision [73–75]. In addition wetting transitions of simple cubic Ising lattices with free surfaces at which surface fields H_1 act have been studied extensively [5, 76–80]. Thus many ingredients that need to be known for a study of droplet formation near wetting transitions are indeed available for the present model. Note that Monte Carlo codes for Ising systems also perform much faster [81] than for off-lattice models. Thus the problem can be studied with efficient use of computer resources. Figures 1, and 2 show snapshot pictures of wall-attached droplets in the lattice gas model, as they are generated and analyzed by our simulations.

In order to provide a stringent test of (4), we extend a method [43, 64, 82–84] where $\gamma_{v\ell}(R)$ is extracted from a study of $\Delta\mu(\rho)$ for different linear dimensions L of the simulation box (applying periodic boundary conditions throughout, in the study addressing homogeneous nucleation) to the case of an $L\times L\times D$ geometry where periodic boundary conditions act only in x and y directions, while at the two $L\times L$ surfaces (which are perpendicular to the z-direction) surface fields H_1 and $-H_1$ act. As it will be described in section 3, the analysis of the function $\Delta\mu$ versus ρ does contain the desired information on $\Delta F^*_{\rm het}$. Of course, as in the bulk [43, 82, 83] one needs to avoid using simulation data which are affected by the 'droplet evaporation/condensation transition' [43, 82, 83, 85–87], which occurs when ρ is too close to ρ_v. In addition, H_1 and L have to be chosen such that transitions where the droplet spreads into a precursor of a wetting film are avoided. (Of course, $H_1 < H_{1\rm w}(T)$ needs

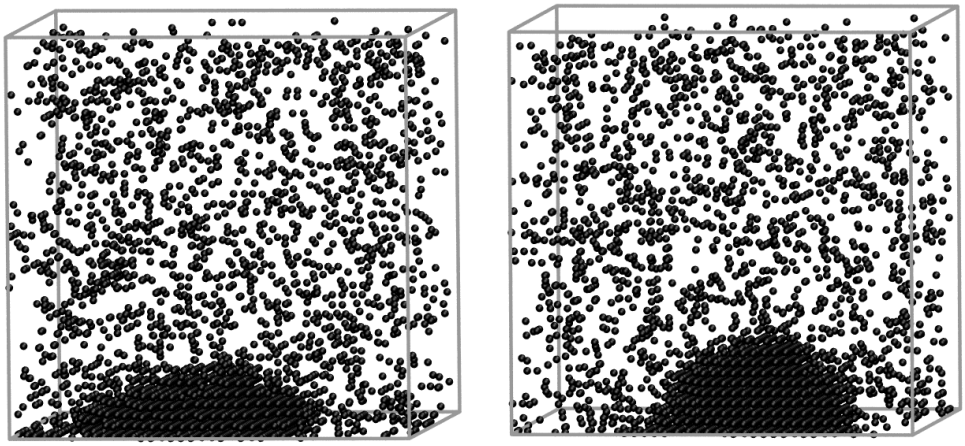

Figure 1. Typical configuration snapshots of systems at $k_B T/J = 3.0$ in the regime where wall-attracted droplets exist in a box with $L = D = 40$. Case (left) refers to $H_1/J = 0.4$ (contact angle $\Theta \approx 58°$) and case (right) to $H_1 = 0$ ($\Theta = 90°$). Occupied lattice sites are highlighted by dots. Lengths are measured in units of lattice spacings and contact angles refer to 'macroscopic' contact angles as derived from (3).

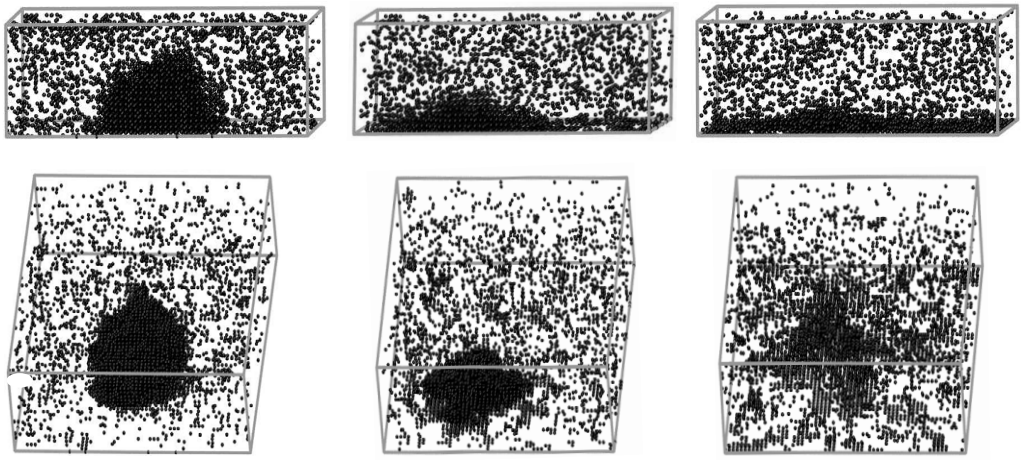

Figure 2. Same as figure 1, but for an elongated geometry ($L = 60$, $D = 20$) and two different views of the same configuration. Systems refer to $H_1 = 0$ ($\Theta = 90°$) left part; $H_1/J = 0.5$ ($\Theta \approx 49°$), middle part; and $H_1/J = 0.7$ ($\Theta \approx 27°$), right part.

to be chosen, $H_{1w}(T)$ denotes the surface field at which in semi-infinite geometry a wetting transition occurs [5, 76–80]). As it will be shown in section 3, accurate estimates of the contact angle Θ as function of H_1 can be easily obtained from a thermodynamic integration method [88–90]. Section 4 then presents our results for $\Delta F^*_{\rm hom}(R^*)$ versus R^*, since previous related work [64] suffers from insufficient statistical accuracy. Section 5 presents the Monte Carlo test of (4), section 6 summarizes our conclusions.

2. Equilibrium of liquid droplets at walls in finite volumes

2.1. Model and general phenomenological considerations

The physical situation which we address in this work is sketched in figure 3(a): we consider a *finite volume* $L \times L \times D$, with periodic boundary conditions in x and y directions, confined by two parallel perfectly flat walls of area $L \times L$. The wall at $z = 0$ favors the liquid (because of a suitably chosen attractive potential between this wall and the fluid particles) and the wall at $z = D$ favors the vapor (because of a suitably chosen repulsive potential between this wall and the fluid particles). The attractive potential needs to be chosen such that (for the considered temperature T less than the critical temperature T_c of the vapor–liquid phase transition in the bulk) the wall at $z = 0$ is incompletely wet (and similarly, the wall at $z = D$ should be incompletely dry).

We now assume that the total density ρ in this system is inside the two-phase region of the bulk, $\rho_v < \rho < \rho_\ell$. We assert that for suitably chosen parameters (ρ, L, D, T and wall potentials) the situation sketched in figure 3(a), where a sphere-cap-shaped droplet covers a spherical surface πr^2 of the substrate) represents a situation of stable equilibrium. The equilibrium can be described by an extension of the lever rule, provided r is of mesoscopic size (much larger than interparticle distances in the fluid)

$$\rho V = \rho'_\ell V_{\rm drop} + (V - V_{\rm drop})\rho'_v. \qquad (7)$$

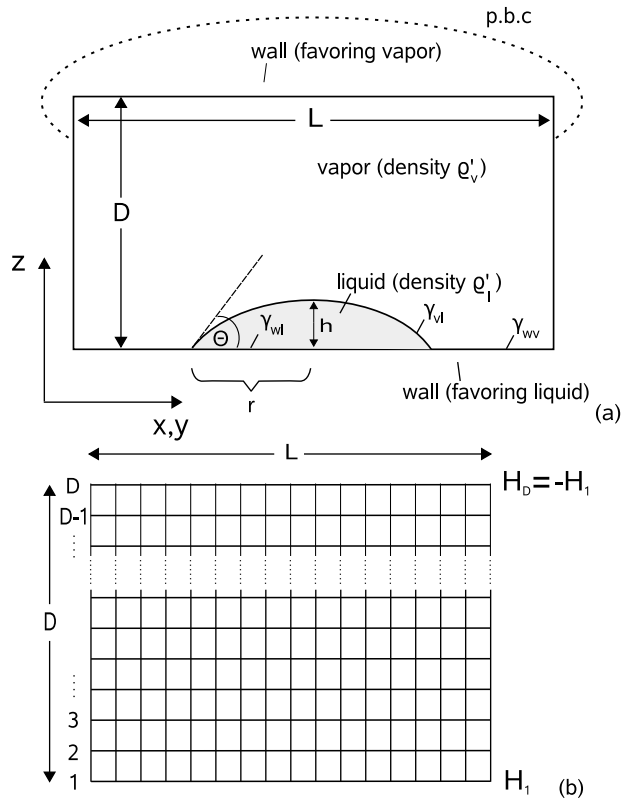

Figure 3. (a) Schematic geometry of the system used to study stable wall-attached droplets in thermal equilibrium. The finite $L \times L \times D$ simulation box has periodic boundary conditions (p.b.c.) in x and y directions, and is confined by an attractive wall (favoring the liquid phase) in the bottom plane ($z = 0$) and by a repulsive wall (favoring the vapor) in the top plane ($z = D$). For suitable average densities ($\rho > \rho_v$) the system is in a two-phase configuration, consisting of a (weakly supersaturated) vapor of density ρ'_v, with $\rho_v < \rho'_v < \rho$, and a sphere-cap-shaped sessile droplet at the lower wall. This droplet is characterized by a height h and contact angle Θ, covering a circle of radius r of the substrate. At the surface area πr^2 the surface tension $\gamma_{w\ell}$ and at the remaining substrate surface $L^2 - \pi r^2$ the surface tension γ_{wv} acts, while the surface tension $\gamma_{v\ell}$ acts on the top surface (of area $\pi(r^2 + h^2)$) of the droplet. (b) Ising model representation of the same geometry as in (a). Using the lattice spacing as a unit of length, we work with D discrete lattice planes in the z-direction, and surface fields act on the planes $n = 1$ (H_1) and $n = D$ ($H_D = -H_1$), respectively.

For a sphere-cap-shaped droplet, the droplet volume $V_{\rm drop}$ is

$$V_{\rm drop} = \frac{\pi h}{6}(3r^2 + h^2), \tag{8}$$

where both radius r and height h can be related to the radius of curvature R and contact angle Θ as

$$r = R\sin\Theta, \qquad h = R(1 - \cos\Theta). \tag{9}$$

The total volume is $V = L^2 D$, and the liquid and vapor densities ρ'_ℓ, ρ'_v in figure 3(a) will (for finite R) differ slightly from the coexistence densities ρ_ℓ, ρ_v due to surface effects. Of course, we do expect that in the limit where $R \to \infty$ (implying also $L \to \infty$, $D \to \infty$ together with R) that $\rho'_\ell \to \rho_\ell$ and $\rho'_v \to \rho_v$, since boundary corrections cannot matter for infinite volumes. The surface free energy of the droplet, relative to the surface with no droplet, is

$$F_{\rm s} = \gamma_{v\ell}\pi(r^2 + h^2) + \pi r^2(\gamma_{w\ell} - \gamma_{\rm wv}). \tag{10}$$

Using Young's equation, (3), and (10) can be rewritten as

$$\begin{aligned} F_{\rm s} &= \gamma_{v\ell}\pi[r^2(1 - \cos\Theta) + h^2] \\ &= \gamma_{v\ell} 4\pi R^2 (1 - \cos\Theta)^2(2 + \cos\Theta)/4 \end{aligned} \tag{11}$$

(for simplicity, line tension corrections are disregarded for the moment).

The idea of the present work now is to study such equilibria as schematically sketched in figure 3(a) by simulation and obtain the total free energy of the system as well as the free energy densities of the vapor and the liquid separately. In this way, the actual effective surface free energy contribution $F_{\rm s}(R, \Theta)$ can be estimated, and the accuracy of (11) for small droplets can be tested.

For simplicity, we continue the discussion not for the general case of a vapor–liquid transition but specialize to the case of an Ising (lattice gas) Hamiltonian, cf figure 3(b).

$$\begin{aligned} \mathcal{H} = &-J\sum_{\langle i,j\rangle} S_i S_j - H\sum_i S_i \\ &- H_1 \sum_{i\in n=1} S_i - H_D \sum_{i\in n=D} S_i. \end{aligned} \tag{12}$$

The lattice sites (i) carry Ising spins $S_i = \pm 1$, J is the exchange constant ($J \equiv 1$ for simplicity) and the first sum goes over all nearest-neighbor pairs of the finite lattice once. (Note that unlike [76–80, 90] we do not consider the case of interactions $J_{\rm s} \neq J$ in the surface planes $n = 1$ and $n = D$, respectively). In the surface planes, each spin has a 'missing neighbor' (since there are no planes $n = 0$ and $n = D + 1$, respectively) but also couples to a 'surface magnetic field' [76–80, 90, 91] H_1 or $H_D = -H_1$, respectively, while all spins couple to the uniform magnetic field H. The connection to the liquid–gas transition discussed so far is made by the standard interpretation of (12) as a lattice gas problem, of course, where S_i translates to a local density ρ_i via

$$\begin{aligned} \rho_i = (1 + S_i)/2, \qquad 2H = \mu - \mu_{\rm coex}, \\ \rho = (1 + \langle S_i\rangle_T)/2. \end{aligned} \tag{13}$$

The coexisting densities in the bulk simply correspond to

$$\rho_v = (1 - m_{\rm coex})/2, \qquad \rho_\ell = (1 + m_{\rm coex})/2, \tag{14}$$

$m_{\rm coex}$ being the absolute value of the spontaneous magnetization ($H = 0$, states with $m \equiv \langle S_i\rangle_T = m_{\rm coex}$ and $m = -m_{\rm coex}$ can exist). In the following, we shall use the 'magnetic terminology' of the Ising model throughout, because it makes the particle–hole symmetry of the lattice gas most transparent.

Figure 4 gives a schematic sketch of the states expected for our system (when L and D are large enough, so that assumptions such as (7) make sense). The lower part shows the thermodynamic potential per spin, $g(m)$, versus m, while the upper part shows the field $H(m)$ versus m. Of course, we have the thermodynamic relation

$$H(m) = (\partial g(m)/\partial m)_T. \tag{15}$$

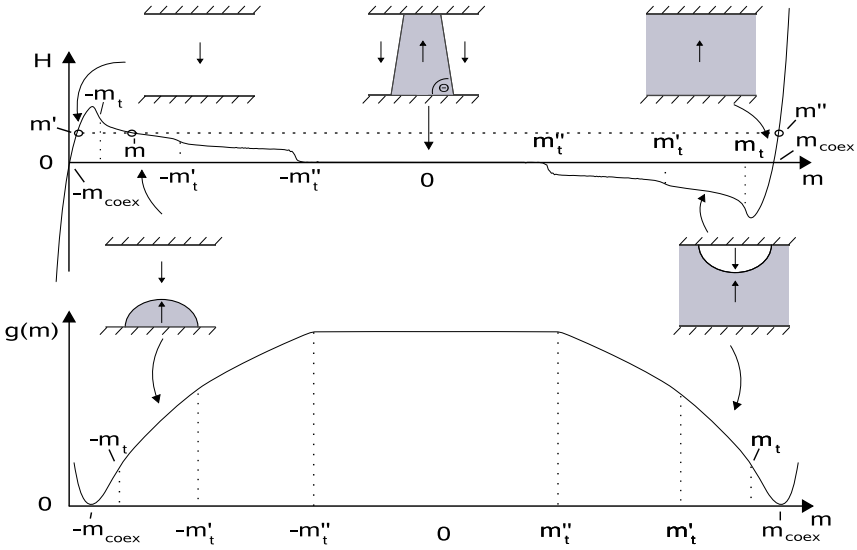

Figure 4. Schematic sketch of an isotherm H versus m (upper part) and associated free energy density per spin $g(m)$ plotted versus m (lower part), for the system of figure 3(b), at a temperature $T < T_c$ and a surface field strength in the incomplete wetting regime $\{H_1 < H_{1w}(T)\}$. The distinct branches separated by transitions (full dots) correspond to the different states of the thin film indicated in the figure: in the regime $-m_{coex} < m < -m_t$ supersaturated vapor occurs, for $-m_t < m < -m'_t$ coexistence between a sphere-cap-shaped droplet plus (slightly supersaturated) vapor occurs, for $-m'_t < m < -m''_t$ coexistence between a cylinder-cap-shaped droplet plus vapor occurs, while for $-m''_t < m < m''_t$ a liquid slab occurs, separated from vapor by flat interfaces which are inclined according to the contact angle (Θ). For positive m the roles of vapor and liquid are reversed. Due to the choice $H_D = -H_1$ the isotherm is strictly antisymmetric around the point $m = 0$, $H = 0$ and $g(m)$ satisfies the symmetry relation $g(-m) = g(m)$. Arrows indicate the orientation of the magnetization in the corresponding Ising spin representation. The dotted horizontal straight line in the upper part indicates that for $H > 0$ three states can occur for the same field, indicated by open circles: a state with magnetization m' with $-m_{coex} < m' < -m_t$, corresponding to the vapor density ρ'_v in figure 3(a); a state with magnetization m with $-m_t < m < -m'_t$, corresponding to the coexistence of this weakly supersaturated vapor with a liquid droplet; and a bulk liquid phase (magnetization $m'' > m_{coex}$, corresponding to the liquid density ρ'_ℓ in figure 3(a)). Note also that $g(m)$ is measured relative to the thermodynamic potential at coexistence, so $g(m_{coex}) = 0$.

Figure 4 suggests that one can distinguish several regions of m, with well-defined separate physical states in these regions, separated by sharp phase transitions. Of course, these sharp phase transitions only exist in an asymptotic sense when L and D both tend to infinity. However this limit is very subtle, since then $m_t \to m_{coex}$ [43, 82, 83, 85, 86], and (noting the normalization $g(m_{coex}) = 0$ for the thermodynamic potential per spin) $g(m) = 0$, for $-m_{coex} \leqslant m \leqslant +m_{coex}$ (while in this regime the total thermodynamic potential $G(m) = L^2 D g(m)$ still tends to infinity, it diverges weaker than proportional to the volume!). For finite L and D, the transitions at $\pm m_t$, $\pm m'_t$ and $\pm m'_t$ are not sharp, but rather exhibit finite size roundings. In [86], it was suggested that this finite size rounding can be described by the 'double Gaussian approximation' and 'equal weight rule', similarly as it applies for first-order transitions in the bulk [92, 93]. Here the details of this rounding are not considered. The linear variation of H versus m drawn for $-m_{coex} < m < -m_t$ and for $m_t < m$ simply corresponds to the linear expansion at coexistence

$$\begin{aligned} m - m_{coex} &= \chi_{coex} H, \qquad \text{near } m = m_{coex}, \quad \text{and} \\ m + m_{coex} &= \chi_{coex} H, \qquad \text{near } m = -m_{coex} \end{aligned} \tag{16}$$

χ_{coex} being the Ising model susceptibility at coexistence. Equation (16) implies a simple quadratic variation of $g(m)$ in this regime,

$$\begin{aligned} g(m) &= \tfrac{1}{2}\chi_{coex}^{-1}(m - m_{coex})^2 \qquad \text{and} \\ g(m) &= \tfrac{1}{2}\chi_{coex}^{-1}(m + m_{coex})^2. \end{aligned} \tag{17}$$

The first of these equations applies near $m = +m_{coex}$ and the second near $m = -m_{coex}$, of course.

A key observation suggested by figure 4 is the possibility that for the same value H of the field three states are possible: a state with (negative) magnetization m', corresponding to the slightly supersaturated vapor of density ρ'_v (figure 3(a)); a state with (positive) magnetization m', corresponding to liquid with density ρ'_ℓ; and a mixed-phase state, at magnetization m (with $-m_t < m < -m'_t$), which is a superposition of these two states, a liquid droplet (with density ρ'_ℓ inside the droplet) and vapor (of density ρ'_v) outside of the droplet. Of course, these considerations assume that the droplet shown in figures 3(a) and 4 is of mesoscopic size: it must be possible to distinguish the 'bulk' region of the droplet from its interfacial region. In figure 4, we have not considered the problem that the interface between liquid and gas has a finite thickness, but this problem is irrelevant in this context: one can define the division between liquid and vapor such that there is neither an excess volume V_{int} nor an excess particle number N_{int} associated with the interface:

$$\begin{aligned} V = V_v + V_\ell, \qquad N = N_v + N_\ell, \qquad V_{int} = 0, \\ N_{int} = 0, \end{aligned} \tag{18}$$

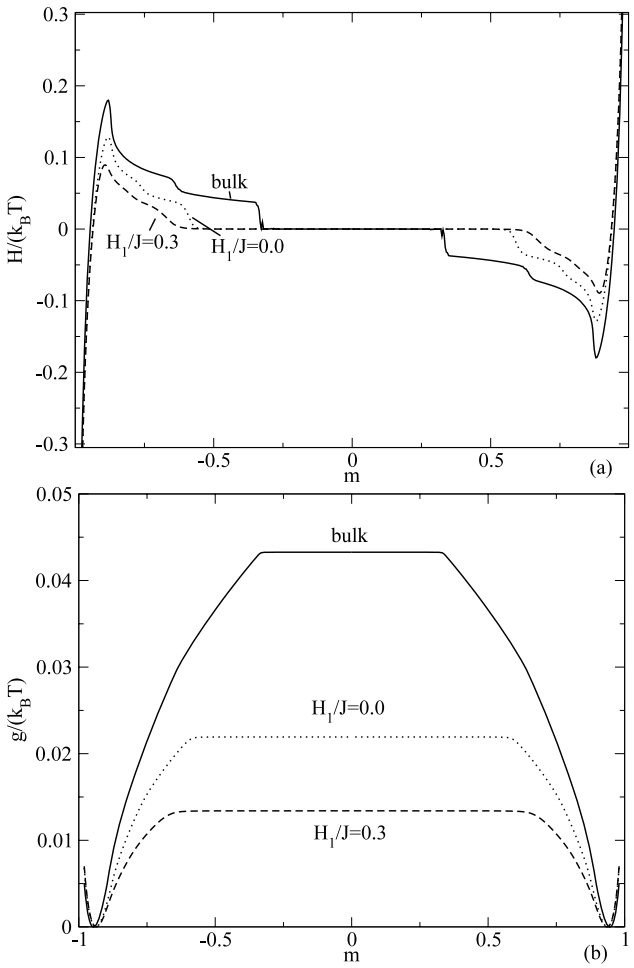

Figure 5. Plot of H versus m (a) and $g(m)$ (b). The chosen temperature is $k_B T/J = 3.0$, $L = D = 20$, and two choices of H_1/J are included, as shown. For comparison, the corresponding bulk data (no surfaces, fully periodic boundary conditions) are included, too.

where V_v, V_ℓ are the volumes taken by vapor and liquid, and N_v, N_ℓ the respective particle numbers (which are related to the corresponding magnetization, using (13) of course). In fact, (18) has already been anticipated by (7). Figure 5 gives an example to show that the isotherms actually observed in the simulation do have the general features postulated in figure 4.

The situation is more subtle when we consider the thermodynamic potential of inhomogeneous states, because then the surface free energy contributions must be considered properly. Equation (17), of course, only describes the bulk part, but does not include a contribution due to the walls in figures 3 and 4 yet. So the actual thermodynamic potential (per lattice site) is, in the state describing the slightly supersaturated vapor,

$$g_{\rm sv}(m) = \tfrac{1}{2}\chi_{\rm coex}^{-1}(m + m_{\rm coex})^2 + (\gamma_{\rm vw} + \gamma_{\ell w})/D \qquad (19)$$

where the dependence of both $\gamma_{\rm vw}, \gamma_{v\ell}$ on H has been neglected. Hence the wall–vapor and wall–liquid surface free energies at bulk phase coexistence are used, as well as the symmetry relation which then holds

$$\gamma_{\rm vw}(H_1) = \gamma_{\ell w}(-H_1) \qquad (20)$$

since the invariance of the Hamiltonian (12), against the transformation

$$\{S_i\}, H, H_1 \to \{-S_i\}, -H, -H_1 \qquad (21)$$

implies for the surface correction to the thermodynamic potential the symmetry $g_{\rm s}(m, H_1) = g_{\rm s}(-m, -H_1)$, which is (20).

For the potential of the state containing the sphere-cap-shaped drop in equilibrium with surrounding supersaturated vapor the ansatz replacing (19) then is

$$g_{\rm drop}(m) = \tfrac{1}{2}\chi_{\rm coex}^{-1}(m' + m_{\rm coex})^2 + (\gamma_{\rm vw} + \gamma_{\ell w})/D + \frac{4\pi R^2 \gamma(R, \Theta)}{L^2 D}. \qquad (22)$$

Note that the first term on the right-hand side of this equation does not involve m but rather m', corresponding to ρ_v', the density that is in equilibrium with a droplet which has the radius of curvature R (figure 3(a)). The last term on the right-hand side represents the surface excess free energy of the sphere-cap-shaped droplet which has a contact angle Θ. According to the classical theory of heterogeneous nucleation,

$$\gamma(R, \Theta) = \gamma_{\ell v} f(\Theta), \qquad (23)$$

with $f(\Theta)$ being given by (4). Clearly we need not make this assumption in (22), and hence allowing for a completely general $\gamma(R, \Theta)$ one can put (23) to a crucial test. When ρ_v' (and hence m') is chosen, the value of R of the sphere cap in equilibrium with its surrounding is also fixed. Varying L and D one can clearly separate the last term on the right-hand side of (22), when $g_{\rm drop}(m)$ is computed from the simulations. Using (7) and (9) (and hence R, given the knowledge of the contact angle Θ) the droplet volume can be directly computed as well. There is no need to geometrically identify the spins belonging to the droplet.

We also note that the fact that the density ρ_v' (magnetization m') in figures 3, and 4 of the vapor coexisting with the droplet is identical to the state with the same value of H and no droplet, is fully consistent with the principle that in equilibrium subsystems are additive. E.g., in figure 3 we can divide the considered system up in a subsystem with $L' < L$ (but the same D) still containing the droplet, and the remaining volume which contains only the supersaturated vapor (at density ρ_v') but no droplet. In the smaller subsystem, $L'^2 D < L^2 D$, hence the contribution of the droplet to $g_{\rm drop}$ in (22) is relatively larger. We can consider a subsystem of total lateral linear dimension L' (connected at this distance with a periodic boundary condition) and should obtain identical results for $f_{\rm s}(R, \Theta)$, as long as the interaction of the droplet with its periodic images remains negligible, and as long as all considered systems stay off from the transitions occurring at $m = -m_{\rm t}$ and $m = -m_{\rm t}'$, respectively.

2.2. The droplet evaporation–condensation transition

While the transition at $m = -m_{\rm t}'$ from sphere-cap-shaped to cylinder-cap-shaped droplets can be found from simple geometrical considerations (using that for large L and D ρ_ℓ'

tends to ρ_ℓ and ρ_v' tends to ρ_v, (7) simply requires that at m_t' the volume of the sphere cap and the volume of the cylinder cap are equal), the droplet evaporation/condensation transition at $m = -m_t$ is more subtle [43, 82, 83, 85, 86]. Since this transition strongly constrains the applicability of our method (in a simulation run it must be ensured that fluctuations where the droplet evaporates and the system jumps to the upper branch of the H versus m curve in figure 4 make negligible contributions to all averages that are taken), it is of interest to discuss this transition more closely. We follow here the treatment given in [86] for the bulk case.

Since we are interested in the asymptotic behavior for large L, D and R, we may insert (23) in (22) and also use (2) for the relation between R and H, i.e.

$$R = \gamma_{v\ell}/(m_{\rm coex} H). \tag{24}$$

The transition point at $m = -m_t$ is located from the condition $g_{sv}(-m_t) = g_{\rm drop}(-m_t)$, cf figure 4, which yields

$$\tfrac{1}{2}\chi_{\rm coex}^{-1}(m_{\rm coex} - m_t)^2 = \tfrac{1}{2}\chi_{\rm coex}^{-1}(m_{\rm coex} - m')^2 + \frac{4\pi\gamma_{v\ell} f(\Theta)}{L^2 D} R^2. \tag{25}$$

Note that at $m = -m_t$ the field H is discontinuous. We expect a jump from $H = H_{t,1}$ in the supersaturated phase with no droplet down to $H = H_{t,2}$ in the state where the droplet coexists with the surrounding vapor. It is convenient to use $H_{t,2}$ as the variable in which all quantities are expressed, since at the transition $R = \gamma_{\ell v}/(m_{\rm coex} H_{t,2})$ and hence (25) becomes

$$\tfrac{1}{2}\chi_{\rm coex}^{-1}(m_{\rm coex} - m_t)^2 = \tfrac{1}{2}\chi_{\rm coex} H_{t,2}^2 + \frac{4\pi\gamma_{\ell v}^3 f(\Theta)}{m_{\rm coex}^2 H_{t,2}^2}\frac{1}{L^2 D}. \tag{26}$$

A second equation for m_t follows from (7)–(9) and (14), namely

$$-m = -m' + (m'' + m')\frac{4\pi R^3 f(\Theta)}{3L^2 D}, \tag{27}$$

where we have used the fact that with the help of (9) the volume of the sphere-cap-shaped drop (8) can be written as $V_{\rm drop} = \frac{4\pi}{3} R^3 f(\Theta)$, $f(\Theta)$ being the function already quoted in (4). Note that due to (16) we can use $m'' + m' = 2m_{\rm coex}$. Hence, at the transition (27) becomes, adding $m_{\rm coex}$ at both sides of (27) and using (16)

$$m_{\rm coex} - m_t = \chi_{\rm coex} H_{t,2} + 2m_{\rm coex}\frac{4\pi}{3}\frac{\gamma_{\ell v}^3 f(\Theta)}{m_{\rm coex}^3 H_{t,2}^3}\frac{1}{L^2 D}. \tag{28}$$

Using (28) in (26) yields a simple algebraic equation for $H_{t,2}$, which readily is solved as

$$H_{t,2}^4 = \frac{8\pi}{3}\frac{\gamma_{\ell v}^3 f(\Theta)}{m_{\rm coex}^2 \chi_{\rm coex}}\frac{1}{L^2 D}. \tag{29}$$

This result constitutes a natural generalization of the corresponding result of [86] for the evaporation–condensation transition in a homogeneous system (which is recovered from (29) if we take $D = L$ and $f(\Theta) = 1$). From $H_{t,2}$ one finds the corresponding magnetization m', $m' = -m_{\rm coex} + \chi_{\rm coex} H_{t,2}$, and from (28) one finds m_t, which yields

$$m_{\rm coex} - m_t = 2\chi_{\rm coex} H_{t,2} = 2(m_{\rm coex} - m'). \tag{30}$$

Since for the branch of $H(m)$ without droplet (16) holds up to the transition point, i.e. $m_{\rm coex} - m_t = \chi_{\rm coex} H_{t,1}$, we immediately conclude that $H_{t,1} = 2H_{t,2}$.

Equations (29) and (30) imply that for constant aspect ratio L/D the same scaling of the critical fields $H_{t,1}$, $H_{t,2}$ and the distance of the transition from the coexistence curve as in the bulk occurs, namely,

$$H_{t,1} = 2H_{t,2} = (m_{\rm coex} - m_t)/(2\chi_{\rm coex}) \propto L^{-3/4}. \tag{31}$$

However, care is necessary in the use of (29) when Θ is small, since then $f(\Theta) \approx \Theta^4/8$ and then (29) shows that $H_{t,2} \propto \Theta$. Clearly, the treatment makes only sense if L satisfies the inequality

$$L \gg 2r = 2R\sin\Theta = 2\gamma_{\ell v}\Theta/(m_{\rm coex} H) \tag{32}$$

which can be rearranged in this limit to give

$$L^2/D \gg \frac{48}{\pi}\gamma_{\ell v}\chi_{\rm coex}/m_{\rm coex}^2. \tag{33}$$

As discussed in [86], near the critical point the combination of quantities appearing on the right-hand side of (33) is related to the correlation length,

$$\gamma_{\ell v}\chi_{\rm coex}/m_{\rm coex}^2 = c\xi_{\rm coex}, \qquad c \approx 0.439. \tag{34}$$

For our treatment to be meaningful, we hence have to require that

$$D \gg \xi_{\rm coex}, \qquad L \gg \xi_{\rm coex}, \quad \text{and} \quad L^2/D \gg \xi_{\rm coex}. \tag{35}$$

3. Estimation of the contact angle in Ising models

When we consider an Ising magnet in a geometry of a very thick film, ($D \to \infty$), the total free energy per spin can be separated into the bulk free energy $f_b(T, H)$ and contributions from the two surfaces [91]

$$f(T, H, H_1, H_D, D) = f_b(T, H) + \frac{1}{D} f_s(T, H, H_1) + \frac{1}{D} f_s(T, H, H_D), \qquad D \to \infty. \tag{36}$$

Here, we consider the thermodynamic limit $L \to \infty$ for the parallel linear dimension. The choice of very large D renders the two surfaces as noninteracting. Just as in the bulk we have the relation for the bulk magnetization $m_b = -(\partial f_b(T, H)/\partial H)_T$, we find the surface layer magnetizations m_1, m_D [91]

$$m_1 = -(\partial f_s(T, H, H_1)/\partial H_1)_T, \qquad m_D = -(\partial f_s(T, H, H_D)/\partial H_D)_T. \tag{37}$$

As is well known, wetting transitions can only occur at bulk phase coexistence [1–5], i.e. $H = 0$ in the Ising model,

but care is necessary to distinguish the sign of the spontaneous magnetization. So we denote by $f_s^{(+)}(T, 0, H_1)$ the limit which results when in (36) the limit $H \to 0^+$ is taken, i.e. a system with a positive spontaneous magnetization, and by $f_s^{(-)}(T, 0, H_1)$ the corresponding result for a system with a negative spontaneous magnetization. In the wet phase of the Ising model, we have a (mesoscopically thick) domain of magnetization adjacent to the surface at $n = 1$, separated by an interface from the domain with the bulk magnetization which take the bulk of the film. Consequently, the surface excess free energy of a wet surface is

$$f_s^{\text{wet}}(T, 0, H_1) = f_s^{(-)}(T, 0, H_1) + \gamma_{v\ell}(T), \qquad (38)$$

while for the non-wet surface it is $f_s^{\text{nonwet}}(T, 0, H_1) = f_s^{(+)}(T, 0, H_1)$, in the case where the bulk spontaneous magnetization is positive. The wetting transition occurs when $f_s^{\text{wet}}(T, 0, H_1) = f_s^{\text{nonwet}}(T, 0, H_1)$, i.e.

$$\gamma_{v\ell}(T) = f_s^{(+)}(T, 0, H_1) - f_s^{(-)}(T, 0, H_1). \qquad (39)$$

In the non-wet situation, Young's equation for the contact angle simply becomes

$$\gamma_{v\ell}(T) \cos\Theta = f_s^{(+)}(T, 0, H_1) - f_s^{(-)}(T, 0, H_1), \qquad (40)$$

consistent with the fact that $\Theta \to 0$ signifies the wetting transition [1–5]. Now it is convenient to make use of the symmetry already noted in (20) and (21) which in the present notation reads

$$f_s^{(-)}(T, 0, H_1) = f_s^{(+)}(T, 0, -H_1), \qquad (41)$$

and which implies that for $H_1 = 0$ the contact angle must be 90°. Making use of (41) we can rewrite (40) as

$$\cos\Theta = [f_s^{(+)}(T, 0, H_1) - f_s^{(+)}(T, 0, H_D)]/\gamma_{v\ell}(T) \qquad (42)$$

where we have also used the choice $H_D = -H_1$. This result suggests to compute the contact angle via a simple thermodynamic integration method,

$$\cos\Theta = [\gamma_{v\ell}(T)]^{-1} \int_0^{H_1} (m_D - m_1)\, \mathrm{d}H_1', \qquad (43)$$

utilizing (37). Thus, one performs a calculation where the surface fields $H_1' < 0$, $H_D' = -H_1' > 0$ are varied for a film with positive magnetization. (By symmetry, one could use a film with negative magnetization as well, then $H_1' > 0$, $H_D' = -H_1' < 0$ is chosen). The interfacial free energy $\gamma_{v\ell}(T)$ can be taken from the results of Hasenbusch and Pinn [74, 75], for instance.

Figure 6 shows the resulting variation of Θ with H_1, using (43) for two system sizes at $k_BT/J = 3.0$, namely a system where $L = D = 40$ and a second system with $L = 100$, $D = 60$. The (second-order) wetting transition for this system has been previously estimated to occur at [76, 77] $H_{1w}(T)/J = 0.83 \pm 0.01$, and the variation of Θ seen in figure 6 is indeed compatible with this estimate. Of course, the purpose of the present work is not to study critical wetting in the Ising model more closely, which would require an extensive analysis of finite size effects near the wetting transition, but rather to obtain Θ as a function of H_1 over a reasonably wide range in the non-wet regime.

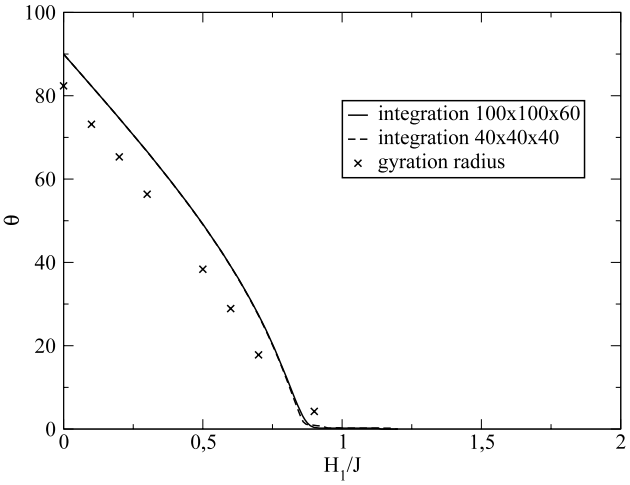

Figure 6. Contact angle Θ plotted versus H_1/J. Full curve is obtained for a system with $L = 100$, $D = 60$, and broken curve for a $L = D = 40$ system. The symbols result from a direct observation of wall-attached droplets, as described in the text, using the droplet gyration radius (crosses). All data refer to $k_BT/J = 3.0$.

It is interesting to test to what extent the 'macroscopic' contact angle, as estimated from the Young equation (42) agrees with the 'microscopic'contact angle extracted from the direct observation of small droplets, as shown in figure 1. As is well known, accurate estimation of contact angles is difficult for both lattice and continuous models. One possibility would be to obtain the density profile of the droplet by averaging over many droplet configurations. However, extracting the contact angle is somewhat ambiguous-the droplet interface is curved for a small droplet, and due to its intrinsic width and its distortion near the wall such estimates are only possible within large error bars [39], and sometimes only qualitative statements are possible [94]. Therefore, we have tried an alternative method: when one assumes a sphere cap shape of the droplet, the contact angle can be written in terms of the parallel ($\langle R_{g,xy}^2 \rangle$) and perpendicular ($\langle R_{g,z}^2 \rangle$) components of the gyration radius as $\cos\Theta = (\langle R_{g,xy}^2 \rangle - 6\langle R_{g,z}^2 \rangle)/(\langle R_{g,xy}^2 \rangle + 2\langle R_{g,z}^2 \rangle)$ These estimates are included in figure 6. However, it is likely that the strong fluctuations in droplet shape occurring for small droplets also imply a systematic error of these estimates.

4. Estimation of the surface free energies of droplets in bulk vapor

As discussed in introduction (section 1), for a test of the predicted formula (4) for the reduction of the free energy barrier at a wall, the knowledge of the barrier ΔF_{hom}^* against homogeneous nucleation in the bulk vapor is needed. Since (2) implies $\Delta F_{\text{hom}}^* = \frac{4\pi}{3} R^{*2} \gamma_{v\ell} = \frac{1}{3} F_s(R^*)$, we need to record the surface free energy $F_s(R) = 4\pi R^2 \gamma_{v\ell}(R)$ of droplets in bulk vapor as a function of the droplet size. Unlike (2), we do not insist on the validity of the capillarity approximation here,

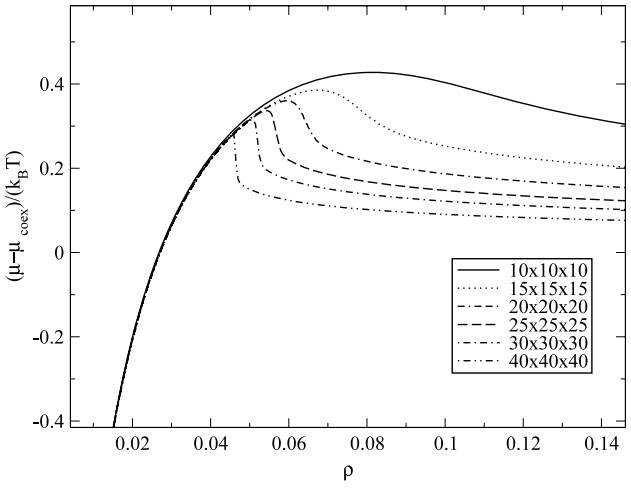

Figure 7. Chemical potential difference $\mu - \mu_{\text{coex}}$ plotted versus ρ at $k_{\text{B}}T/J = 3.0$, for the three-dimensional lattice gas model in the bulk. Cubic $L \times L \times L$ simulation boxes with periodic boundary conditions are used, for a broad range of L, as indicated.

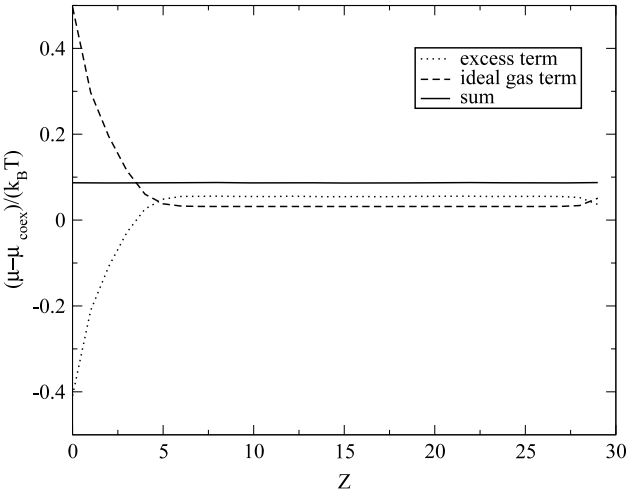

Figure 8. Chemical potential as a function of distance from the attractive wall. At $z = 0$ a droplet is located at the wall. The configuration shown is from a system with $L = D = 30$, $H_1/J = 0.4$, and $\rho = 0.06$ at temperature $k_{\text{B}}T/J = 3.0$.

but allow for a more general form of a vapor–liquid interfacial tension $\gamma_{v\ell}(R)$ that may depend on the droplet radius R, as done in [43] for a Lennard-Jones fluid. In principle, our approach may allow another test of (6).

The method to obtain $F_{\text{s}}(R)$ is the same as described in section 2.1: the only change is that the terms $(\gamma_{vw} + \gamma_{\ell w})/D$ in (19) and (22) need to be omitted, and $\Theta = \pi$ throughout (as in the case for a system with walls in the complete drying regime, where a droplet formed in the vapor does not want to touch the walls).

Figure 7 shows the 'raw data' of our study, namely a plot of $\mu - \mu_{\text{coex}}$ versus the density ρ, for $L \times L \times L$ systems with periodic boundary conditions, for a broad range of linear dimensions L, as indicated. For obtaining the chemical potential of the lattice gas as a function of density, an adaptation of the Widom particle insertion method [95, 96] to the lattice model proved to be convenient.

$$H = \frac{k_{\text{B}}T}{2} \ln \frac{2}{V - M - 2} \sum_{M_-} \exp(-\beta \Delta E_{M+2}). \qquad (44)$$

Here, ΔE_{M+2} is the energy to flip a spin from the magnetization M to $M + 2$. $\sum_{M_-}$ is the sum over all lattice positions with $S_i = -1$ and $V = L \times L \times D$ the number of spins in the system. This equation is in principle only valid in a region of constant density. If one is interested in a system with varying density, one has to restrict the measurement to regions of constant density except for systems in equilibrium where one can average over the whole system. For Lennard-Jones systems the chemical potential is typically separated into two parts: the ideal gas term and the excess term. Analogously we can write

$$\begin{aligned} H &= \frac{k_{\text{B}}T}{2} \ln \left(\frac{2V}{V - M - 2} \right) \\ &\quad + \frac{k_{\text{B}}T}{2} \ln \left(\frac{1}{V} \sum_{\text{M}_-} \exp(-\beta \Delta E_{\text{M}+2}) \right) \\ &= H_{\text{id}} + H_{\text{exc}}. \end{aligned} \qquad (45)$$

In figure 8 we plot both terms as a function of distance from the attractive wall. Note that even though a droplet is present the total chemical potential is constant as expected from equilibrium considerations. More details can be found in [97]. The data in figure 7 are compatible with the earlier results found in [64], but the latter data are considerably less precise, as expected. Very similar to the corresponding data for Lennard-Jones fluids [43, 83], one can distinguish three regimes: for ρ near ρ_v (remember that $\mu = \mu_{\text{coex}}$ at ρ_v), this size dependence of the isotherms is negligibly small. The anomaly that exists in the regime $0.04 < \rho < 0.09$ (for the choices of L shown in figure 7) is a remnant of the droplet evaporation/condensation transition, rounded by finite size: rather than finding a sharp kink with a vertical part of the isotherm, we find a smooth curve with a rounded maximum. The position of this maximum shifts to smaller density as L increases, and at the same time, it becomes sharper. Qualitatively, these findings agree with the considerations about the finite size rounding of the droplet evaporation/condensation transition presented in [86]. We do not attempt to analyze this behavior further. For such a study considerably larger values of L would be required, as it was found for the Lennard-Jones fluids [43, 83]. In any case, the behavior seen in figure 7 is strikingly similar to corresponding data [43, 83, 84] for Lennard-Jones fluids, strengthening our belief that the present work is not suffering severely from any possible lattice artifacts. A notable feature of the isotherms in figure 7 is their pronounced curvature in the regime of the vapor without droplet, unlike the strictly linear variation which was drawn in figure 4 for simplicity. This also means that the linear variation of the bulk grand-canonical potential per unit volume, used in (1)

$$\begin{aligned} \Delta p &= p'_\ell - p'_v \\ &= p_\ell + \rho_\ell(\mu - \mu_{\text{coex}}) - p_v - \rho_v(\mu - \mu_{\text{coex}}) \\ &= \Delta\mu(\rho_\ell - \rho_v) \end{aligned} \qquad (46)$$

does not hold yet for the parameters chosen for our numerical work. However, since the more general form of (1) and (2) is

$$R^* = 2\gamma_{v\ell}/[\Delta p],$$
$$\Delta F^*_{\rm hom} = \frac{16\pi}{3}[\gamma^3_{v\ell}/(\Delta p)^2] = \frac{4\pi}{3}R^{*^2}\gamma_{v\ell}, \tag{47}$$

the result that $\Delta F^*_{\rm hom} = (1/3)F_{\rm s}(R^*)$ holds irrespective of whether the linear expansion around the coexistence curve is an accurate approximation to the actual isotherms in the vapor region or not.

The data for the isotherms $\mu-\mu_{\rm coex}$ versus ρ, in the regime of densities where we always have coexistence of a droplet with surrounding vapor (without being affected by the droplet evaporation/condensation transition for too small ρ, and the droplet/cylinder transition for too large ρ) yield information on the droplet surface free energy, $F_{\rm s}(R) = 4\pi R^2\gamma(R)$, cf (22). Here, the thermodynamic potential $g_{\rm drop}(m)$ is found from thermodynamic integration, using (13)–(15)

$$g(m) = \int_{-m_{\rm coex}}^{m} {\rm d}\tilde{m}\, H(\tilde{m}), \tag{48}$$

and (48) is also used to estimate $g_{sv}(m')$, rather than using the quadratic approximation in (19), since the latter is equivalent to the linear variation of (16), and we know already that the latter is inaccurate in the regime of interest, as noted above. From (22), we hence conclude (in our case $D = L$, no free surface effects and no contact angle enters)

$$F_{\rm s}(R) = L^3[g_{\rm drop}(m) - g_{\rm sv}(m')]. \tag{49}$$

At a given value of $H = (\mu - \mu_{\rm coex})/2$ in the suitable regime, we can read off both m and m' (and also m'', from the part of the isotherm near $m = +m_{\rm coex}$, not shown here). The radius R belonging to this value is then inferred from (27) which reduces in the bulk case to

$$m' - m = (m'' + m')(4\pi/3)(R/L)^3. \tag{50}$$

Thus, an explicit observation of the droplet in particular spin configurations is not required. Problems related to the precise identification which up-spins should be counted as part of the droplet [98] hence do not even arise. We note, that 'physical droplets' [98] in the Ising model should not (at least for temperatures near the bulk critical point) be defined as clusters of up-spins connected by nearest-neighbor bonds. Rather one should use the 'Swendsen–Wang' [99] clusters, where bonds between parallel spins are only placed with a probability $P = 1 - \exp(-J/k_{\rm B}T)$ to define connectivity of spins belonging to a cluster. However, we here disregard this problem, leaving an analysis of nucleation close to criticality to later work.

An important aspect of (49) and (50) is that the same R and associated free energy $F_{\rm s}(R)$ can be obtained for different choices of L. This fact can be used as a stringent test of the self-consistency of our procedure. Indeed, the pieces of the curves for $F_{\rm s}(R)$ versus R extracted from the different box linear dimensions L in figure 10 superimpose precisely, compellingly proving the accuracy of our data.

It is also interesting to compare our findings for $F_{\rm s}(R)$ to the prediction of the capillarity approximation, $F_{\rm s}(R) = 4\pi R^2\gamma_{v\ell}$, using the estimates [74, 75]

$$\gamma_{v\ell}/(k_{\rm B}T) = 0.434(1) \qquad (k_{\rm B}T/J = 3.0),$$
$$\gamma_{v\ell}/(k_{\rm B}T) = 0.0981(1) \qquad (k_{\rm B}T/J = 4.0). \tag{51}$$

One can see from figure 10 that in the region where $100 < F_{\rm s}(R)/k_{\rm B}T < 600$ the relative deviations between the capillarity approximation are relatively small, at least for $k_{\rm B}T/J = 3$. For $k_{\rm B}T/J = 4$ there seems to be an almost constant offset. Only for $F_{\rm s}(R)$ smaller than $100\ k_{\rm B}T$ significant deviations gradually become important. Note that the theory outlined in section 2 loses its validity when R becomes too small (in this case L also needs to be small, to avoid problems with the droplet evaporation/condensation transition, and then the droplet in the simulation box is affected by interaction with its own periodic images). Such finite size effects are not a physically important limitation of our study. For free energy barriers $\Delta F^*_{\rm hom} \approx (5-20)k_{\rm B}T$ one needs to describe nucleation as a kinetic process. Prefactors in the nucleation rate become important, and nucleation events can no longer be considered to be independent of each other: The growing droplet creates a depletion zone around itself interacting with the depletion zones of other droplets, and one observes a gradual transition from nucleation to spinodal decomposition [14, 15].

5. Monte Carlo results for the surface free energies of wall-attached droplets

As a first test of our concepts outlined in section 2.1, we show for a small system ($L = 20$, $D = 20$, $H_1 = 0$) a measurement of the isotherm for the chemical potential and the corresponding potential $g(m)$, figure 5. Apart from finite size roundings, one can see all the features of the theoretical curves shown in figure 4. Figure 9(a) now shows data analogous to those shown in figure 7, but now in presence of walls (still using $H_1 = 0$). When we compare these data to the corresponding results from the bulk (figure 7), we see a qualitatively very similar behavior, with one important exception: there is now a distinct dependence of the branch corresponding to the vapor without droplet on the system size. A closer examination shows, that $\mu - \mu_{\rm coex}$ in this regime depends strongly on D (as expected, due to the term $(\gamma_{\rm vw} + \gamma_{\ell w})/D$ in $g(m)$, cf (19) and (22)) but not on L, as it should be. In 'magnetic notation', cf (36), we note that the magnetization of the system contains corrections which are called the 'surface excess magnetization' [91],

$$m = -(\partial f/\partial H)_{T,H_1,H_D} \tag{52}$$
$$= m_b + \frac{1}{D}m_{\rm s}(T, H, H_1) + \frac{1}{D}m_{\rm s}(T, H, H_D)$$

and these surface excess magnetizations $m_{\rm s}$ are picked up in the curves $\mu - \mu_{\rm coex}$ versus ρ. It is also interesting to take a direct look at typical configuration snapshots corresponding to these states (figures 1 and 2). These snapshot pictures already indicate that one must also pay careful attention to finite size

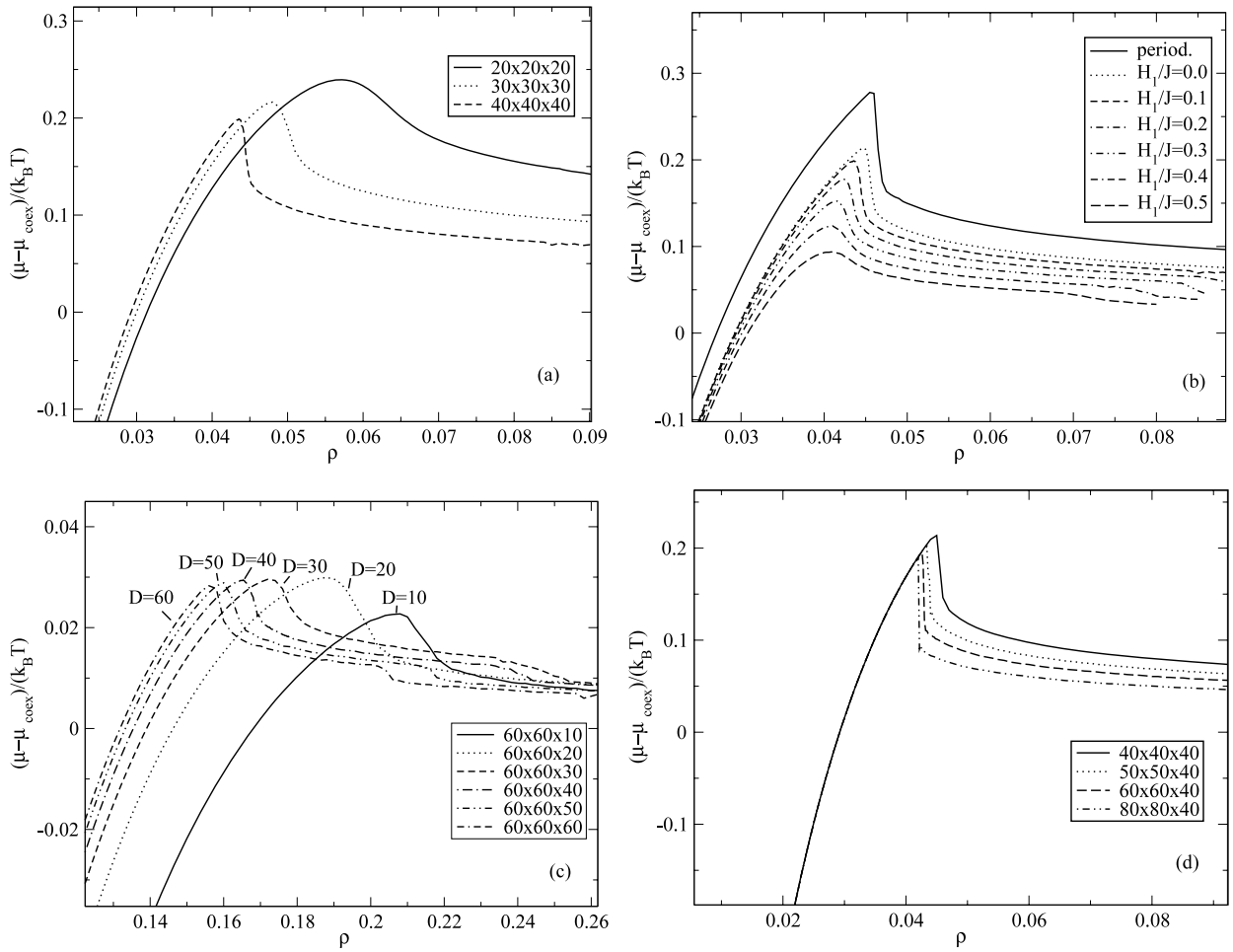

Figure 9. Plot of $\mu - \mu_{\rm coex}$ versus ρ for $k_{\rm B}T/J = 3.0$ and $H_1 = 0$ for three different lattice sizes (a) and for a system of size $40 \times 40 \times 40$ where H_1 is varied. (b) Part (c) shows data for $k_{\rm B}T/J = 4.0$ and systems $60 \times 60 \times D$ for various D, choosing $H_1 = 0.0$. (d) shows systems with $L \times L \times 40$ and varying L for $k_{\rm B}T/J = 3.0$ and $H_1 = 0.0$.

effects associated with the lateral linear dimension L of the box due to the proximity of the second-order wetting transition when Θ is small: the system may undergo fluctuations into states which are the dominating equilibrium configurations for $H_1 > H_{1\rm w}(T)$. For small Θ, in the regime where for $H_1 < H_{1\rm w}(T)$ one expects to observe a droplet, rather a state is observed where this droplet has spread out into a precursor of a wetting layer. Thus we have disregarded data for $L = 20$ throughout and used data for $L = 30$ only for $H_1/J \leqslant 0.4$. For $H_1/J \geqslant 0.6$, also $L = 40$ was too small, and $L = 60$ or 80 had to be used. These configurations were used to determine the gyration radius of the droplets from which another estimate for Θ can be extracted, see [100]. As expected, such estimates of Θ from the direct observation of rather small droplets are less reliable.

Using data such as shown in figure 9, we can conclude that the excess $m' - m$ for two states with the same field H at the ascending branch (m') and descending branch (m) of an isotherm, away from the droplet evaporation–condensation transition and from the sphere-cap–cylinder-cap transition, differ just by the excess order parameter due to the (sphere-cap-shaped) droplet, $m' - m = (m'' + m')V_{\rm drop}/(L^2 D)$, analogous to (50) for the bulk case. Using $V_{\rm drop} = (4\pi R^3/3) f(\Theta)$, we relate $m' - m$ to the droplet radius of curvature, assuming again a sphere cap shape of the droplet (and using the appropriate contact angle from figure 6). The associated differences in the thermodynamic potential yield the droplet surface free energy $F_{\rm s}(R, \Theta) = L^2 D[g_{\rm drop}(m) - g(m')]$, in analogy to (49). Since this method ignores a possible systematic error, if the contact angle Θ differs from its 'macroscopic' value (figure 6) because of a line tension effect, we have also used an alternative method, where R was taken from the corresponding bulk measurement at the same value of H (note that there is a unique relation between R and H, beyond the validity of the classical nucleation theory). From this estimate for R and the estimate for $V_{\rm drop}$ one obtains an alternative estimate for Θ (which differs from the estimate from figure 6 only slightly). Consequently, slightly different estimates for $F_{\rm s}(R, \Theta)$ result. Since the statistical errors for this method seem to be somewhat larger, the resulting estimates were not shown here.

Figure 11 now presents the central results of our paper, the surface free energy of the droplets $F_{\rm s}(R, H_1)$ plotted versus the droplet radius R (using the data in figure 6 where Θ is given as a function of H_1, $F_{\rm s}(R, H_1)$ is readily converted into $F_{\rm s}(R, \Theta)$, of course). One can see, that the walls indeed cause a dramatic reduction of the free energy barrier, qualitatively as expected

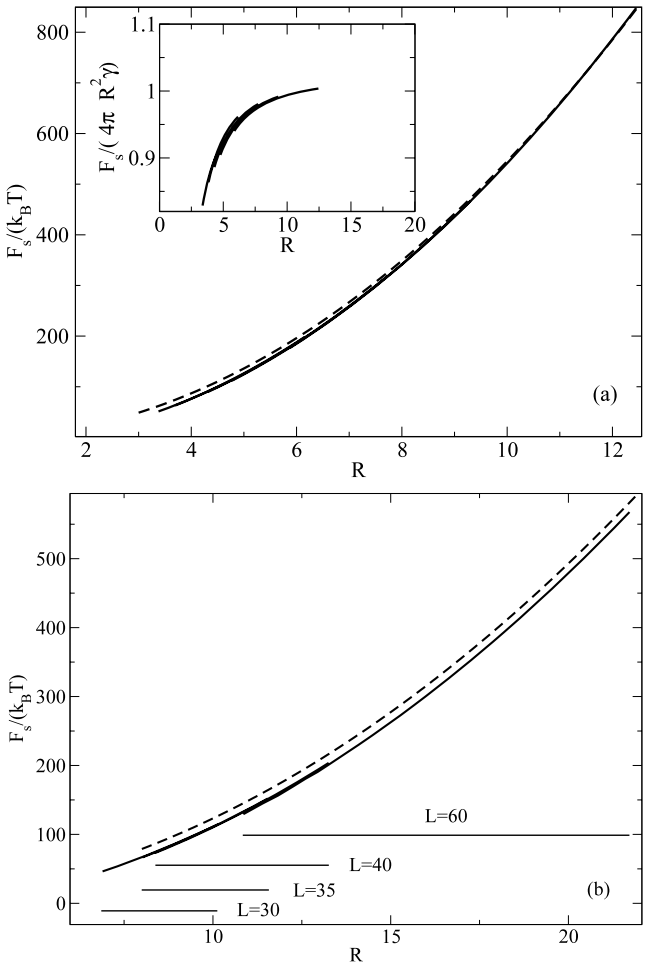

Figure 10. Surface free energy $F_s(R)/(k_BT)$ plotted versus droplet radius R, extracted from the data as shown in figure 7 by the method explained in section 2.1. Two temperatures are shown, $k_BT/J = 3.0$ (a) and $k_BT/J = 4.0$ (b). Broken curves show the prediction of the capillarity approximation, $F_s(R) = 4\pi R^2\gamma_{v\ell}$, where $\gamma_{v\ell}$ is the interface tensions of flat interfaces (51). The straight lines (b) show the ranges of the different linear dimensions L of the $L \times L \times L$ systems used. Inset in part (a) shows that the relative deviation from the classical capillarity approximation increases strongly with decreasing R.

from (4). In order to test this prediction, (4), quantitatively, we have used the theoretical factor $f(\Theta)$ in (4), to construct the function

$$F_s(R, \Theta) = F_s(R) f(\Theta) \tag{53}$$

where $F_s(R)$ is the surface energy of droplets in the bulk (i.e., the simulation result obtained for periodic boundary conditions). One sees that (49) can indeed explain the simulation results almost quantitatively. There is, however, a systematic offset (of the order of 10–20 k_BT) which depends on the droplet radius (figure 12). It is tempting to attribute this deviation to a line tension effect (figure 13), cf (5). I.e., (53) is replaced by $F_s(R, \Theta) \equiv F_s(R) f(\Theta) + 2\pi R \sin(\Theta)\tau$, where τ is the line tension. The resulting line tension is found to be negative for $H_1 = 0$ and its absolute magnitude decreases when H_1 increases towards $H_{1w}(T)$. Of course, the present data become more and more inaccurate for H close to $H_{1w}(T)$, due to the strong fluctuations associated with the critical wetting transition, and finite size effects associated with too small values chosen for L and D: hence, the analysis of how the line tension behaves near critical wetting in the Ising model is clearly beyond the scope of the present study. One may ask the question to what extent the line tension itself depends on the radius $r = R \sin\Theta$ of the circle enclosing the sphere cap at the substrate surface. To answer this question, we have also estimated τ from $g(m)$ in slab configurations with $m = 0$ (figure 4). Within our statistical accuracy, no significant dependence on r was found, however.

6. Conclusions

In this paper we have introduced a method to study the excess free energy of sessile liquid droplets, attached to a flat wall in the regime of incomplete wetting of the wall as it is exposed to a saturated vapor. This method is based on a study of the chemical potential as a function of density, for finite $L \times L \times D$ simulation boxes, where periodic boundary conditions are used in x and y directions, while the wall at $z = D$ is chosen such that it prefers the vapor phase. It is shown, by theoretical arguments which are verified by Monte Carlo simulations, that in the finite-sized box there is for each (sufficiently large) value of L a region of densities ρ where the (stable) thermodynamic equilibrium between the sessile liquid droplet and the surrounding vapor (which in comparison with the saturated vapor under coexistence conditions in the bulk) has a (slightly) enhanced density ρ' and that this equilibrium in the finite systems can also be described by the lever rule. Since the droplet and the surrounding vapor have the same chemical potential (μ) as the corresponding bulk phases (ρ', ρ''), one can obtain both the total particle number excess due to the droplet and its volume from observations of these densities, ρ, ρ' and ρ''. As the thermodynamic potential for all states can be found by thermodynamic integration of the relation $\mu(\rho) = (\partial g(\rho, T)/\partial\rho)_T$, the excess free energy of the droplet results, without the need to identify which atoms belong to the droplet in a particular configuration, and which belong to the vapor. As is well known, such 'cluster criteria' to define droplets from atomistic configurations suffer in principle from some arbitrariness in their definition. While this problem does not hamper simulations at low enough temperatures, where impressive simulations of large sessile droplets have been performed [101], near the vapor–liquid critical point such studies of droplets based on neighborhood criteria between atoms are hardly feasible.

We have demonstrated the feasibility of our approach for the simplest possible model of a fluid in three dimensions, the nearest-neighbor lattice gas model on the simple cubic lattice. Varying a short range attractive potential due to the wall acting on the particles (which in the Ising spin representation of the lattice gas is nothing but a 'surface magnetic field' H_1), the contact angle Θ can easily be varied from $\Theta = 90°$ to $0°$ (choosing conditions where the wetting transition of the model is second order). Exploiting the special symmetries of the model, Θ can be found explicitly with very good accuracy. For the mesoscopic droplet sizes studied, only rather rough

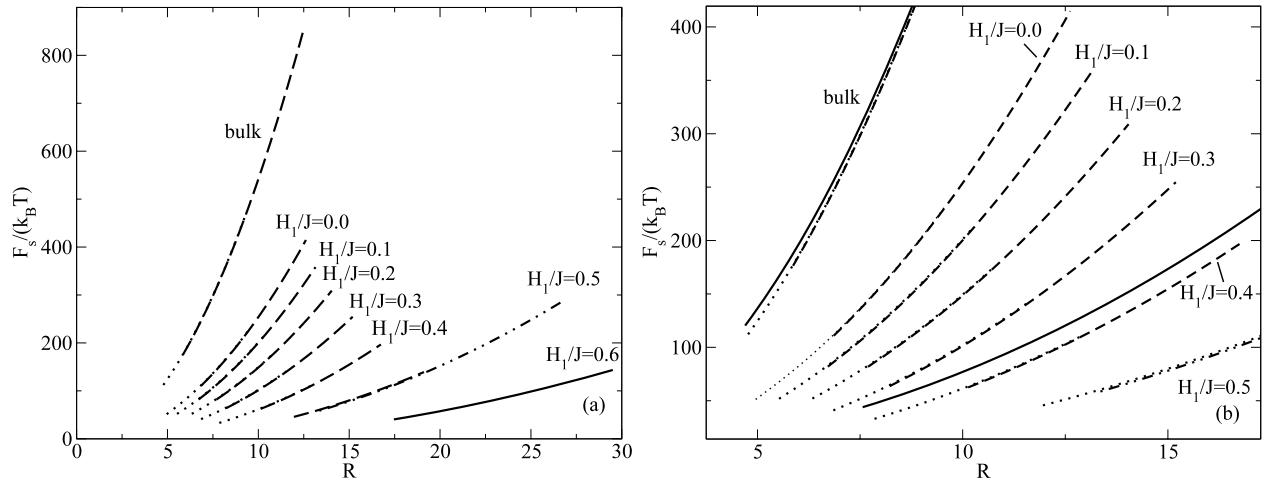

Figure 11. (a) Plot of $F_s(R, H_1)/(k_BT)$ versus R for $k_BT/J = 3.0$ and a broad range of values for H_1. (b) Same as (a), but magnified region from $R = 4$ to 16. Dotted lines are results from $30 \times 30 \times 30$ systems, dashed lines from $40 \times 40 \times 40$ systems, dashed–dotted line for a $60 \times 60 \times 20$ system ($H_1/J = 0.5$), and continuous line ($H_1/J = 0.6$) for a $50 \times 50 \times 20$ system. For the bulk system and for $H_1/J = 0.4$ we also plotted the theoretical prediction (continuous) $4\pi R^2\gamma_{v\ell}/(k_BT)$ and $4\pi R^2\gamma_{v\ell}/(k_BT)\, f(\Theta)$, respectively (b).

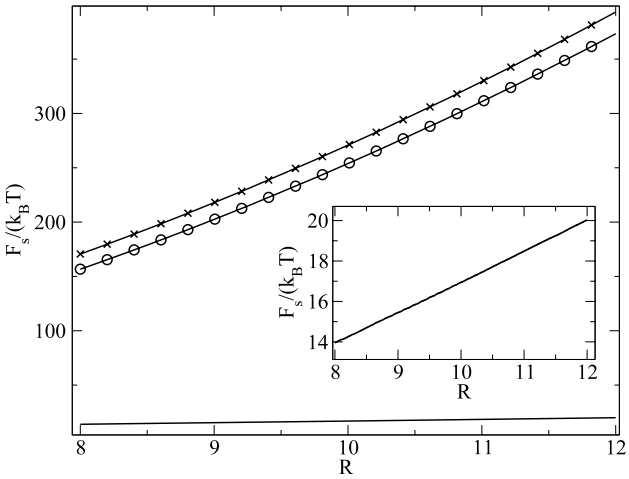

Figure 12. (a) Plot of $F_s(R, \Theta)$ as defined in (49), versus the droplet radius R, for $H_1/J = 0$ where $\Theta = \pi/2$, at $k_BT/J = 3.0$ for a $40 \times 40 \times 40$ system. Crosses show the prediction of the theory that $F_s(R, \Theta = \pi/2) = F_s(R)/2$ in this case, while circles show the actual data for wall-attached droplets, as found in figure 11. The third line without symbols (also shown in the inset) is the difference between the predicted (crosses) and observed results (circles).

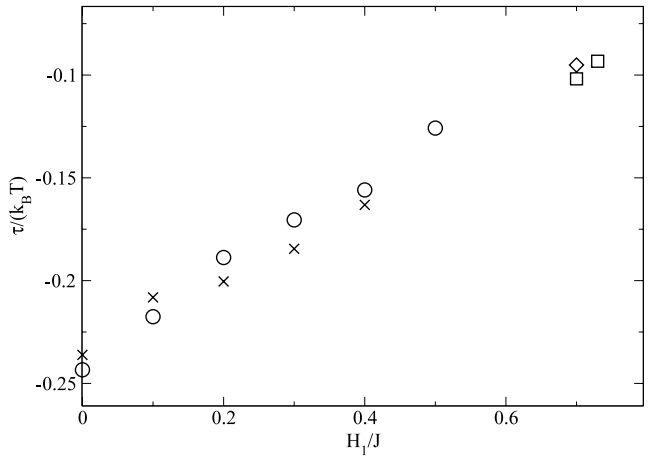

Figure 13. Plot of τ/k_BT versus H_1/J for $k_BT/J = 3.0$. Crosses are data from $30 \times 30 \times 30$ boxes, circles data from $40 \times 40 \times 40$ boxes, while diamonds are data for $60 \times 60 \times 10$ systems, and squares data for $80 \times 80 \times 10$ systems. (For the three rightmost points, the theoretical prediction for $F_s(R$, bulk) was used.)

estimates of Θ are possible from direct observation of the droplets, as expected.

Since the surface excess free energy of the droplets $F_s(R, \Theta)$ has been obtained for a wide range of Θ and values for the droplet radius of curvature with very good accuracy, the formula of Turnbull predicting the corresponding reduction $f(\Theta)$ of the rate of heterogeneous nucleation ΔF^*_{het} at walls in comparison with the rate of homogeneous nucleation, ΔF^*_{hom}, could be tested, since $f(\Theta) = \Delta F^*_{het}/\Delta F^*_{hom} = F(R, \Theta)/F_s(R)$, where $F_s(R)$ is the surface excess free energy of spherical droplets in the bulk. We find that this relation is reasonably accurate, apart from a correction due to the line tension τ. The dependence of the line tensions as function of H_1/J has been estimated. In this way, the first systematic test of the classical theory of heterogeneous nucleation at flat walls near wetting transitions could be performed. In view of the subtle problem of separating contributions of contact lines from the interface contributions, noted in [33], we note that we associate a unit volume with each lattice site, and hence the area of an interface running at $\Theta = \pi/2$ across our system (figure 3(b)) is defined as DL, although the geometric distance between the planes $n = 1$ and $n = D$ is $D - 1$ lattice spacings only.

Having established this methodology for a very simple lattice model, it will be desirable to consider extensions to off-lattice models such as Lennard-Jones fluids, as well as to consider the non-equilibrium dynamics of droplets, caused by change of external conditions (e.g., temperature or pressure quenching experiments). We hope to report on such extensions in the future.

Acknowledgments

We are grateful to the Deutsche Forschungsgemeinschaft (DFG) for support in the framework of the priority program SPP1296, project Bi314/19. We would like to acknowledge computing time at the ZDV cluster in Mainz and at the Jülich supercomputing center.

References

[1] De Gennes P G 1985 *Rev. Mod. Phys.* **58** 827
[2] Sullivan D E and Telo da Gama M M 1986 *Fluid Interfacial Phenomena* ed ed C A Croxton (New York: Wiley) p 45
[3] Dietrich S 1988 *Phase Transitions and Critical Phenomena* vol XII, ed C Domb and J L Lebowitz (New York: Academic) p 1
[4] Schick M 1990 *Liquids at Interfaces* ed J Charvolin, J F Joanny and J Zinn-Justin (Amsterdam: North-Holland) p 415
[5] Binder K, Landau D P and Müller M 2003 *J. Stat. Phys.* **110** 1411
[6] Volmer M and Weber A 1926 *Z. Chem. Phys.* **119** 277
[7] Becker R and Döring W 1935 *Ann. Phys.* **24** 719
[8] Frenkel J 1955 *Kinetic Theory of Liquids* (New York: Dover)
[9] Feder J, Russell K C, Lothe J and Pound G M 1966 *Adv. Phys.* **15** 117
[10] Langer J S 1967 *Ann. Phys.* **41** 108
[11] Langer J S 1969 *Ann. Phys.* **54** 258
[12] Zettlemoyer A C (ed) 1969 *Nucleation* (New York: Dekker)
[13] Abraham F F 1974 *Homogeneous Nucleation Theory* (New York: Academic)
[14] Binder K and Stauffer D 1976 *Adv. Phys.* **25** 343
[15] Binder K 1987 *Rep. Prog. Phys.* **50** 783
[16] Oxtoby D W 1991 *Liquids, Freezing, and the Glass Transition* ed J P Hansen, D Levesque and J Zinn-Justin (Amsterdam: North-Holland) p 145
[17] Kashchiev D 2000 *Nucleation: Basic Theory with Applications* (Oxford: Butterworth-Heinemann)
[18] Balibar S and Villain J 2006 *Nucleation, C. R. Phys.* **7** fascicule 9–10 (special issue)
[19] Young T 1805 *Phil. Trans. R. Soc.* **85** 65
[20] Turnbull D and Fisher J C 1949 *J. Chem. Phys.* **17** 71
[21] Turnbull D 1950 *J. Appl. Phys.* **21** 1022
[22] Turnbull D 1950 *J. Chem. Phys.* **18** 198
[23] Gibbs J W 1961 *The Scientific Papers* vol 1 (New York: Dover)
[24] Boruvka L and Neumann A W 1977 *J. Chem. Phys.* **66** 5464
[25] Rowlinson J S and Widom B 1982 *Molecular Theory of Capillarity* (Oxford: Oxford University Press)
[26] Indekeu J O 1994 *Int. J. Mod. Phys.* B **8** 309
[27] Widom B 1995 *J. Phys. Chem.* **99** 2803
[28] Li D and Steigmann D J 1996 *Colloids Surf.* A **116** 25
[29] Bieker T and Dietrich S 1998 *Physica* A **252** 85
[30] Getta T and Dietrich S 1998 *Phys. Rev.* E **57** 655
[31] Brinkmann M, Kierfeld J and Lipowsky R 2005 *J. Phys.: Condens. Matter* **17** 2349
[32] Djikaev Y 2005 *J. Chem. Phys.* **123** 184704
[33] Schimmele L, Napiorkowski M and Dietrich S 2007 *J. Chem. Phys.* **127** 164715
[34] Gretz R D 966 *J. Chem. Phys.* 1 **45** 3160
[35] Navascues G and Tarazona P 1981 *J. Chem. Phys.* **75** 2441
[36] Swain P S and Lipowsky R 1998 *Langmuir* **14** 6772
[37] Rosso R and Virga E G 2004 *J. Phys. A: Math. Gen.* **37** 3989
[38] Guzzardi L, Rosso R and Virga E G 2006 *Phys. Rev.* E **73** 021602
[39] Milchev A and Binder K 2001 *J. Chem. Phys.* **114** 8610
[40] Tolman R C 1949 *J. Chem. Phys.* **17** 333
[41] Anisimov M A 2007 *Phys. Rev. Lett.* **98** 35702
[42] Ten Wolde P R and Frenkel D 1998 *J. Chem. Phys.* **109** 9901
[43] Schrader M, Virnau P and Binder K 2009 preprint
[44] Fladerer A and Strey R 2006 *J. Chem. Phys.* **124** 164710
[45] Castleman A W 1979 *Adv. Colloid Interface Sci.* **10** 13
[46] Curtius J 2006 *C. R. Phys.* **7** 1027
[47] Swain P S and Lipovsky R 1998 *Langmuir* **14** 6772
[48] Ralston J, Popescu M and Sedov R 2008 *Annu. Rev. Mater. Res.* **38** 23
[49] Quéré D 2008 *Annu. Rev. Mater. Res.* **38** 71
[50] Biloni H 1983 *Physical Metallurgy* ed R W Cahn and P Haasen (Amsterdam: North-Holland) p 477
[51] Bykov T V and Zeng X C 2002 *J. Chem. Phys.* **117** 1851
[52] Talanquer V and Oxtoby D W 1996 *J. Chem. Phys.* **104** 1483
[53] Talanquer V and Oxtoby D W 2001 *J. Chem. Phys.* **114** 2793
[54] Ustinov E A and Do D D 2005 *J. Phys. Chem.* B **109** 11653
[55] Bykov T V and Zeng X C 2006 *J. Chem. Phys.* **125** 144515
[56] Sear R P 2005 *J. Phys. Chem.* B **110** 4985
[57] Sear R P 2006 *Phys. Rev. Lett.* **97** 065701
[58] Auer S and Frenkel D 2003 *Phys. Rev. Lett.* **91** 015703
[59] Cacciuto A, Auer S and Frenkel D 2004 *Nature* **428** 404
[60] Dijkstra M 2004 *Phys. Rev. Lett.* **93** 108303
[61] Cacciuto A and Frenkel D 2005 *Phys. Rev.* E **72** 041604
[62] Sear R P 2007 *J. Phys.: Condens. Matter* **19** 033101
[63] Binder K and Müller-Krumbhaar H 1974 *Phys. Rev.* B **9** 2194
[64] Furukawa H and Binder K 1982 *Phys. Rev.* A **26** 556
[65] Stauffer D, Coniglio A and Heermann D W 1982 *Phys. Rev. Lett.* **49** 1299
[66] Shneidman V A, Jackson K A and Beatty K M 1999 *J. Chem. Phys.* **111** 6932
[67] Shneidman V A, Jackson K A and Beatty K M 1999 *Phys. Rev.* B **30** 3579
[68] Stauffer D 1999 *Int. J. Mod. Phys.* C **10** 809
[69] Pan A C and Chandler D 2004 *J. Phys. Chem.* B **108** 19681
[70] Maibaum L 2008 *Phys. Rev. Lett.* **101** 256102
[71] Neuhaus T and Hager J S 2003 *J. Stat. Phys.* **113** 47
[72] Baxter R J 1982 *Exactly Solved Models in Statistical Mechanics* (London: Academic)
[73] Ferrenberg A M and Landau D P 1991 *Phys. Rev.* B **44** 5081
[74] Hasenbusch M and Pinn K 1993 *Physica* A **192** 343
[75] Hasenbusch M and Pinn K 1994 *Physica* A **203** 189
[76] Binder K and Landau D P 1988 *Phys. Rev.* B **37** 1745
[77] Binder K, Landau D P and Wansleben S 1989 *Phys. Rev.* B **40** 6971
[78] Binder K, Landau D P and Ferrenberg A M 1995 *Phys. Rev.* E **51** 2823
[79] Binder K, Evans R, Landau D P and Ferrenberg A M 1996 *Phys. Rev.* E **53** 5023
[80] Schulz B J, Binder K and Müller M 2005 *Phys. Rev.* E **71** 046705
[81] Landau D P and Binder K 2005 *A Guide to Monte Carlo Simulation in Statistical Physics* 2nd edn (Cambridge: Cambridge University Press)
[82] Binder K and Kalos M 1980 *J. Stat. Phys.* **22** 363
[83] MacDowell L G, Virnau P, Müller M and Binder K 2004 *J. Chem. Phys.* **120** 5293
[84] Virnau P, Müller M, MacDowell L G and Binder K 2004 *New J. Phys.* **6** 7
[85] Biskup M, Chayes L and Kotecky R 2002 *Europhys. Lett.* **60** 21
[86] Binder K 2003 *Physica* A **319** 99
[87] Nussbaumer A, Bittner E, Neuhaus T and Janke W 2006 *Europhys. Lett.* **75** 716
[88] Binder K and Landau D P 1992 *Phys. Rev.* B **46** 4844
[89] Müller M and Binder K 1998 *Macromolecules* **31** 8323
[90] Albano E V and Binder K 2009 *J. Stat. Phys.* at press
[91] Binder K and Hohenberg P C 1972 *Phys. Rev.* B **6** 3461
[92] Binder K and Landau D P 1984 *Phys. Rev.* B **30** 1477
[93] Borgs C and Kotecky R 1990 *J. Stat. Phys.* **61** 79

[94] Wang H, Gould H and Klein W 2007 *Phys. Rev.* E **76** 031604
[95] Widom B 1963 *J. Chem. Phys.* **39** 2808
[96] Widom B 1982 *J. Phys. Chem.* **86** 869–72
[97] Winter D 2009 *Diplomarbeit, Johannes Gutenberg-Universität* Mainz, unpublished
[98] Binder K 1976 *Ann. Phys.* **98** 390
[99] Swendsen R H and Wang J S 1987 *Phys. Rev. Lett.* **58** 87
[100] Ivanov V A, Martemyanova J A, Müller M, Paul W and Binder K 2009 *J. Phys. Chem.* B **113** 3653
[101] Webb E B III, Grest G S and Hoyt J J 2005 *Acta Mater.* **53** 3163